MIT Libraries | DSpace@MIT

MIT Open Access Articles

On-chip chalcogenide glass waveguide-integrated mid-infrared PbTe detectors

The MIT Faculty has made this article openly available. ***Please share*** how this access benefits you. Your story matters.

Citation: Han, Z. et al. "On-Chip Chalcogenide Glass Waveguide-Integrated Mid-Infrared PbTe Detectors." Applied Physics Letters 109, 7 (August 2016): 071111 © 2016 Author(s)

As Published: http://dx.doi.org/10.1063/1.4961532

Publisher: American Institute of Physics (AIP)

Persistent URL: http://hdl.handle.net/1721.1/111848

Version: Final published version: final published article, as it appeared in a journal, conference proceedings, or other formally published context

Terms of Use: Article is made available in accordance with the publisher's policy and may be subject to US copyright law. Please refer to the publisher's site for terms of use.

Massachusetts Institute of Technology

AIP | Applied Physics Letters

On-chip chalcogenide glass waveguide-integrated mid-infrared PbTe detectors

Z. Han, V. Singh, D. Kita, C. Monmeyran, P. Becla, P. Su, J. Li, X. Huang, L. C. Kimerling, J. Hu, K. Richardson, D. T. H. Tan, and A. Agarwal

Citation: Applied Physics Letters **109**, 071111 (2016); doi: 10.1063/1.4961532
View online: http://dx.doi.org/10.1063/1.4961532
View Table of Contents: http://scitation.aip.org/content/aip/journal/apl/109/7?ver=pdfcov
Published by the AIP Publishing

Articles you may be interested in

On-chip mid-infrared gas detection using chalcogenide glass waveguide
Appl. Phys. Lett. **108**, 141106 (2016); 10.1063/1.4945667

CdS/PbSe heterojunction for high temperature mid-infrared photovoltaic detector applications
Appl. Phys. Lett. **104**, 121111 (2014); 10.1063/1.4869752

Responsivity enhancement of mid-infrared PbSe detectors using CaF2 nano-structured antireflective coatings
Appl. Phys. Lett. **104**, 021109 (2014); 10.1063/1.4861186

Study of sensitization process on mid-infrared uncooled PbSe photoconductive detectors leads to high detectivity
J. Appl. Phys. **113**, 103102 (2013); 10.1063/1.4794492

Infrared p-n -junction diodes in epitaxial narrow gap PbTe layers on Si substrates
J. Appl. Phys. **85**, 3364 (1999); 10.1063/1.369685

Reuse of AIP Publishing content is subject to the terms at: https://publishing.aip.org/authors/rights-and-permissions. Download to IP: 18.101.8.134 On: Tue, 23 Aug 2016 02:17:21

On-chip chalcogenide glass waveguide-integrated mid-infrared PbTe detectors

Z. Han,[1,a)] V. Singh,[1] D. Kita,[1] C. Monmeyran,[1] P. Becla,[2] P. Su,[1] J. Li,[3] X. Huang,[4] L. C. Kimerling,[1] J. Hu,[1] K. Richardson,[5] D. T. H. Tan,[6] and A. Agarwal[1,2]
[1]*Department of Materials Science and Engineering, Massachusetts Institute of Technology, Cambridge, Massachusetts 02139, USA*
[2]*Materials Processing Center, Massachusetts Institute of Technology, Cambridge, Massachusetts 02139, USA*
[3]*The Key Laboratory of Optoelectronic Technology and System, Education Ministry of China, Chongqing University, Chongqing 400044, China*
[4]*School of Precision Instruments and Optoelectronics Engineering, Tianjin University, Tianjin 300072, China*
[5]*CREOL, The College of Optics and Photonics, University of Central Florida, Orlando, Florida 32816, USA*
[6]*Photonics Devices and Systems Group, Singapore University of Technology and Design, Singapore 487372, Singapore*

(Received 20 May 2016; accepted 11 August 2016; published online 18 August 2016)

We experimentally demonstrate an on-chip polycrystalline PbTe photoconductive detector integrated with a chalcogenide glass waveguide. The device is monolithically fabricated on silicon, operates at room-temperature, and exhibits a responsivity of 1.0 A/W at wavelengths between 2.1 and 2.5 μm. *Published by AIP Publishing.* [http://dx.doi.org/10.1063/1.4961532]

Detection of infrared (IR) radiation is key to many technical applications including night vision,[1] chemical sensing,[2,3] and medical diagnostics.[4] Traditional IR photodetectors assume free-space geometry. Recently, miniaturization enabled by microphotonic fabrication technology has led to the development of waveguide-integrated photodetectors. Compared to their free-space counterparts, waveguide integrated devices typically decouple the optical absorption path from the carrier transit path, which reduces response time in the case of photovoltaic detectors and enhances gain in the case of photoconductive detectors. The small active volume of waveguide-integrated detectors also improves the signal-to-noise ratio (SNR) by suppressing the generation-recombination noise. Waveguide-integrated detectors based on Ge[5] and III–V materials[6] have been demonstrated in the near-IR telecommunication bands and their performance advantages have been well established. Although waveguide-integrated mid-infrared (MIR) detectors are essential components for mid-infrared (MIR) system-on-a-chip platforms such as spectroscopic sensors,[7] they are much less explored due to the limited material choices. III–V materials and HgCdTe widely used in free-space MIR detectors[1] require epitaxial growth on a lattice-matched substrate and therefore integration on silicon often resorts to a hybrid bonding approach: for example, integration of GaInAsSb detectors on silicon waveguides was demonstrated via adhesive bonding.[8,9]

Lead chalcogenides represent a promising alternative material system for MIR detection.[10,11] In particular, polycrystalline PbTe can be deposited by thermal evaporation directly on a variety of substrates including silicon and has been explored as a candidate for a low-cost silicon-integrated MIR detector solution.[12–14] In addition, our prior work shows that fast oxygen diffusion along the grain boundaries enhances the optical response of the PbTe material by creating spatial charge separation and thereby increasing the carrier lifetime.[14,15] In this paper, we demonstrate a waveguide-integrated PbTe detector monolithically integrated on a silicon substrate and operating at room temperature.

The device uses a 4 in. silicon wafer with a 3 μm thick thermal oxide layer as the starting substrate. All the thin films for device fabrication (PbTe, Sn, and $Ge_{23}Sb_7S_{70}$ glass) are deposited by thermal evaporation used in previously reported protocols.[15,16] A PbTe layer is deposited first, followed by a 300 nm thick Sn contact layer with the $Ge_{23}Sb_7S_{70}$ (GeSbS) waveguide layer on top. We choose $Ge_{23}Sb_7S_{70}$ chalcogenide glass as the waveguide material given its superior chemical stability and compatibility with PbTe materials.[17]

Two sample layouts are used to examine the performance of PbTe detectors: (1) A free space sample consisting of a 650 nm thick PbTe layer with Sn contacts of 0.5 mm spacing patterned using a shadow mask and without the glass waveguide layer. It is used to characterize the material property of PbTe. (2) An integrated sample, with a 100 nm thick and 40 μm long PbTe layer, followed by Sn contacts with 7 μm spacing and an 800 nm thick single-mode GeSbS waveguide on top. The integrated sample is patterned by a lift-off process.[16] The cross-sectional schematic of the integrated device is shown in Figure 1(a).

The structure of the chip is illustrated in Figure 1(b). Light is first coupled into a 2 μm wide GeSbS waveguide. A multimode interferometer (MMI) structure splits the light into two arms that gradually increase to a 5 μm width to improve alignment tolerance between the PbTe layer and the waveguide. The upper arm delivers light into PbTe where most of the light is absorbed. The lower arm, without the PbTe layer, is used for alignment. Figure 1(c) shows the SEM image at 45° view. At the interface of the detector/non-detector section, a clear boundary can be observed due to the abrupt change of the waveguide height. To evaluate the device design at the detector section, we use the Film Mode Matching (FMM) method in FIMMWAVE (PhotonDesign) to simulate the mode propagation,[18] as shown in Figure 2. TM-polarized light from the laser is coupled into the waveguide from the left side

a)Author to whom correspondence should be addressed. Electronic mail: zhaohong@mit.edu.

Reuse of AIP Publishing content is subject to the terms at: https://publishing.aip.org/authors/rights-and-permissions. Download to IP: 18.101.8.134 On: Tue, 23 Aug 2016 02:17:21

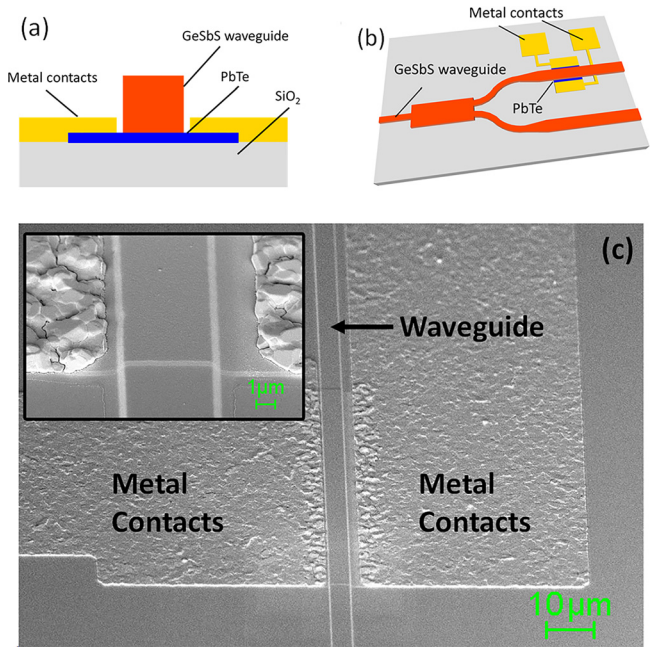

FIG. 1. (a) A schematic cross-sectional view of the integrated MIR detector (not to scale). The thickness of the PbTe layer is 100 nm (blue region) and the width is 13 μm. The width of the waveguide is 5 μm and the height is 800 nm. Metal contact spacing is 7 μm, which means that they are 1 μm away from the waveguide. Underneath the waveguide is 3 μm SiO_2. (b) A schematic representation of the chip design. An MMI structure splits the light into two arms. The lower arm is used for alignment. The upper arm delivers light to the PbTe detector (blue region). Both arms adiabatically increase in width from 2 μm to 5 μm. The PbTe layer and Sn contacts lie underneath the waveguide. (c) A 45° view SEM image of the MIR device.

of the figure. Despite the cross-sectional profile change at the interface, the coupling efficiency from the fundamental TM mode in the glass waveguide to the hybrid TM mode at the detector section is 94% with only about 4% reflections. Coupling into the PbTe strip-loaded mode is minimal (<1%) due to the large effective index and modal profile mismatch. Parasitic absorption by the Sn contacts is less than 0.1% according to the simulation. The decay length of the hybrid mode in the detector section is 16.7 μm.

Sample 1 is sealed in an IR-transparent glass chamber with a thermoelectric cooler (TEC) and a responsivity measurement is subsequently performed at −60 °C. IR light from a white light source passes through a monochromator and directly illuminates the chip. The contacts are wire-bonded to a source measurement unit (SMU) to obtain the I–V curve of the device at different wavelengths. Data are gathered at −60 °C to decrease the dark current (since the optical power

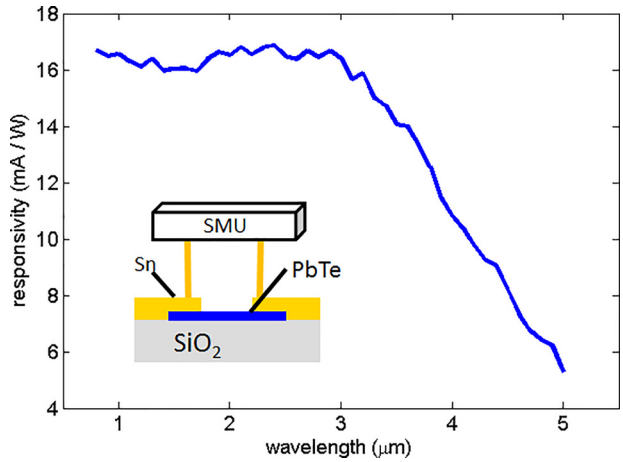

FIG. 3. Response of sample 1 at different wavelengths at 213 K (−60 °C). The bias is 10 V. The spacing between contacts is 0.5 mm. The response drops after 3 μm as the photon energy is close to the band gap of PbTe. The inset is a schematic of sample 1. Sn contacts are wire bonded to a source measurement unit (SMU) to measure the I–V curve.

from the monochromator is much weaker than the laser used for sample 2, we need to decrease the dark current to improve the signal to noise ratio).

The wavelength-dependent responsivity of sample 1 under 10 V bias is shown in Figure 3. We measure the photoconductivity signal in the wavelength range of 0.8–5 μm in the PbTe film. This is consistent with our prior measurement results.[14]

For the integrated sample (sample 2), the PbTe absorption measurement is performed at room temperature using a device characterization set-up as shown in Figure 4. A tunable Cr^{2+}:ZnS/Se laser (2.0–2.5 μm, IPG Photonics) is first coupled to an aspheric lens (C037TME-D, Thorlabs) and then focused into the waveguide. Light from the waveguide output is collected by an IR camera for imaging as well as intensity measurement in the alignment arm. A source measurement unit (Keithley 2401 SMU) is connected to the metal contacts on the chip via two probes to measure the I–V curves.

Sample 2 is measured at room temperature. Optical power coupled into the detector is estimated by subtracting the power loss due to fiber/lens coupling from the total input laser power. Based on the data shown in Figure 5, we calculated the responsivity to be about 1.0 A/W at 2250 nm wavelength. Wavelength-dependent responsivity from 2.1 μm to 2.5 μm wavelengths is plotted in Figure 6. Within our measurement error, the responsivity remains roughly constant throughout this range, which is consistent with the trend shown in Figure 3.

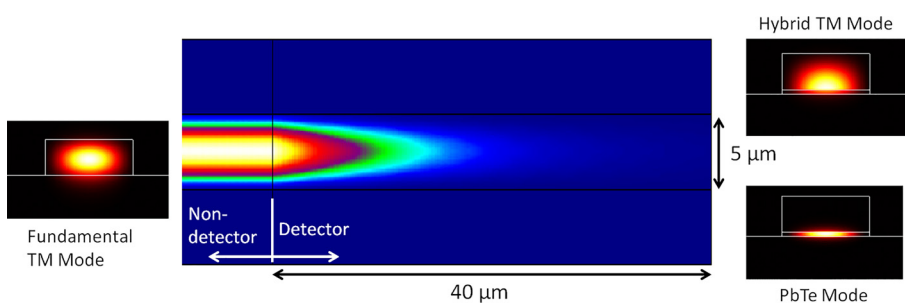

FIG. 2. Simulation results of mode propagation in the PbTe detector (top view). Coupling efficiency from the fundamental TM mode at the non-detector section (mode shape is shown on the left) into the hybrid TM mode at the detector section (shown on the top right) is 94%. Totally less than 1% of the power is coupled into the PbTe mode (example shown on the bottom right). The absorption length in the detector section is 16.7 μm.

Reuse of AIP Publishing content is subject to the terms at: https://publishing.aip.org/authors/rights-and-permissions. Download to IP: 18.101.8.134 On: Tue, 23 Aug 2016 02:17:21

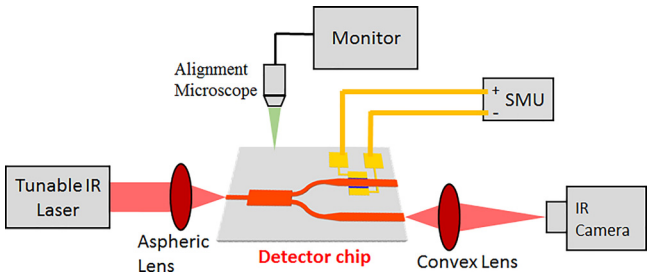

FIG. 4. A schematic representation of the experimental set-up used to characterize the performance of PbTe detectors.

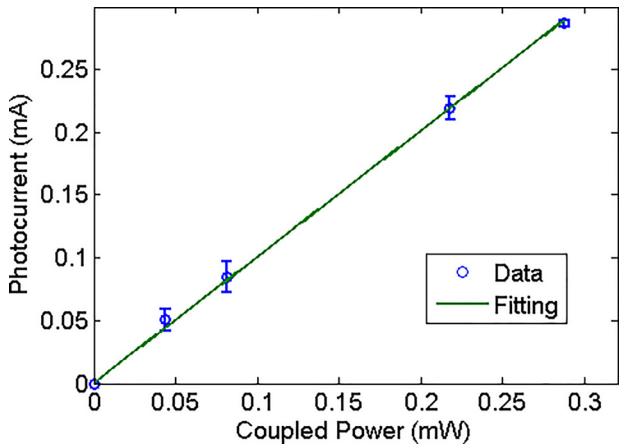

FIG. 5. Photocurrent change as a function of optical power for the integrated device at room temperature and a fixed wavelength of 2250 nm under a bias of 10 V. Responsivity calculated from curve fitting is 1.0 A/W.

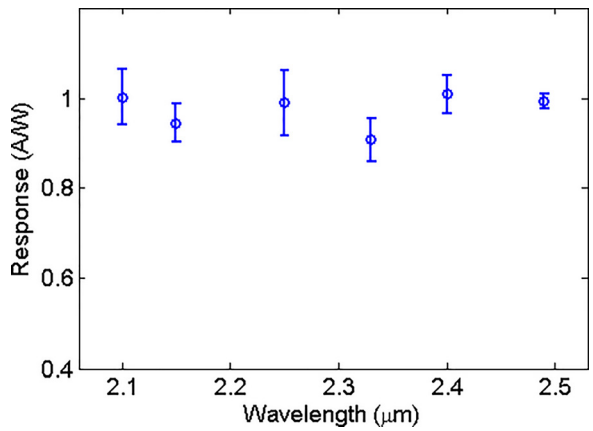

FIG. 6. Uniform responsivity of the integrated detector as a function of wavelength (room temperature).

The error bars associated with the data shown in Figures 5 and 6 are due to the misalignment caused by mechanical vibration of the sample stage. Resistivity of sample 2 (dark) is 1.27 Ω cm. The theoretical responsivity at 2.25 μm, assuming unity absorption efficiency and unity photoconductive gain, is about 1.8 A/W. Our device therefore exhibits a photoconductive gain of 0.59 taking into account the simulated 94% optical absorption efficiency. This figure is consistent with the carrier lifetime and transit time estimated based on the device geometry and Hall carrier mobility. The Johnson noise spectral density calculated from the dark resistance of our device is 8.6×10^{-13} A/Hz$^{1/2}$, which is much larger than the generation-recombination noise (about 1×10^{-19} A/Hz$^{1/2}$ based on Hall effect measurements). Since current flowing through a photoconductor does not have shot noise,[19] Johnson noise limited detectivity of this device is therefore 2×10^{12} cm Hz$^{1/2}$/W.

The results above demonstrate the viability of using polycrystalline PbTe materials for on-chip integrated MIR detection. Further improvement can be made by (1) cooling down the system to decrease the Johnson noise which limits our SNR; (2) using an optical coupler to improve the coupling efficiency to PbTe; and (3) alloy PbTe with SnTe (band gap $\sim$ 0.19 eV) to create smaller band gap materials and extend the detection range.[20]

In conclusion, we demonstrate a room-temperature MIR waveguide-integrated PbTe photodetector. The responsivity is about 1.0 A/W at the 2.1–2.5 μm MIR regime. This platform provides a promising low-cost planar detector solution for MIR lab-on-a-chip devices.

Funding from the Ministry of Defense, Singapore, DOE-NNSA Grant No. DE-NA0002509, and Defense Threat Reduction Agency Grant No. HDTRA1-13-1-0001 are gratefully acknowledged. This work made use of the MRSEC Shared Experimental Facilities at MIT, supported by the National Science Foundation under Award No. DMR-1419807.

[1]A. Rogalski, Opto-Electron. Rev. **20**(3), 279–308 (2012).
[2]R. Soref, Nat. Photonics **4**(8), 495–497 (2010).
[3]P. Werle, F. Slemr, K. Maurer, R. Kormann, R. Mücke, and B. Jänker, Opt. Lasers Eng. **37**(2), 101–114 (2002).
[4]S. Hocde, O. Lore, O. Sire, C. Boussard-Ple, B. Bureau, B. Turlin, J. Keirsse, P. Leroyer, and J. Lucas, J. Biomed. Opt. **9**(2), 404–407 (2004).
[5]D. Ahn, C.-Y. Hong, J. Liu, W. Giziewicz, M. Beals, L. C. Kimerling, J. Michel, J. Chen, and F. X. Kärtner, Opt. Express **15**(7), 3916–3921 (2007).
[6]A. W. Fang, R. Jones, H. Park, O. Cohen, O. Raday, M. J. Paniccia, and J. E. Bowers, Opt. Express **15**(5), 2315–2322 (2007).
[7]Z. Han, P. Lin, V. Singh, L. Kimerling, J. Hu, K. Richardson, A. Agarwal, and D. Tan, Appl. Phys. Lett. **108**(14), 141106 (2016).
[8]N. Hattasan, A. Gassenq, L. Cerutti, J.-B. Rodriguez, E. Tournié, and G. Roelkens, IEEE Photonics Technol. Lett. **23**(23), 1760–1762 (2011).
[9]A. Gassenq, N. Hattasan, L. Cerutti, J. B. Rodriguez, E. Tournié, and G. Roelkens, Opt. Express **20**(11), 11665–11672 (2012).
[10]J. M. Margarit, G. Vergara, V. Villamayor, R. Gutierrez-Alvarez, C. Fernandez-Montojo, L. Teres, and F. Serra-Graells, IEEE J. Solid-State Circuits **50**(10), 2394–2405 (2015).
[11]T. Komissarova, D. Khokhlov, L. Ryabova, Z. Dashevsky, and V. Kasiyan, Phys. Rev. B **75**(19), 195326 (2007).
[12]J. Wang, T. Zens, J. Hu, P. Becla, L. C. Kimerling, and A. M. Agarwal, Appl. Phys. Lett. **100**(21), 211106 (2012).
[13]J. Wang, J. Hu, P. Becla, A. M. Agarwal, and L. C. Kimerling, Opt. Express **18**(12), 12890–12896 (2010).
[14]J. Wang, J. Hu, P. Becla, A. M. Agarwal, and L. C. Kimerling, J. Appl. Phys. **110**(8), 083719 (2011).
[15]J. Wang, J. Hu, X. Sun, A. M. Agarwal, L. C. Kimerling, D. R. Lim, and R. Synowicki, J. Appl. Phys. **104**(5), 053707 (2008).
[16]J. Hu, V. Tarasov, A. Agarwal, L. Kimerling, N. Carlie, L. Petit, and K. Richardson, Opt. Express **15**(5), 2307–2314 (2007).
[17]K. Richardson, L. Petit, N. Carlie, B. Zdyrko, I. Luzinov, J. Hu, A. Agarwal, L. Kimerling, T. Anderson, and M. Richardson, J. Nonlinear Opt. Phys. Mater. **19**(1), 75–99 (2010).
[18]V. Singh, T. Zens, J. Hu, J. Wang, J. D. Musgraves, K. Richardson, L. C. Kimerling, and A. Agarwal, Sens. Actuators, B **185**, 195–200 (2013).
[19]G. D. Boreman, *Infrared Detectors and Systems* (Wiley-Interscience, 1996).
[20]I. Melngailis and T. Harman, Appl. Phys. Lett. **13**(5), 180–183 (1968).

Reuse of AIP Publishing content is subject to the terms at: https://publishing.aip.org/authors/rights-and-permissions. Download to IP: 18.101.8.134 On: Tue, 23 Aug 2016 02:17:21